Role of boron and phosphorus in enhanced electrocatalytic oxygen evolution by nickel borides and nickel phosphides

Justus Masa[†], Corina Andronescu[†], Hendrik Antoni[‡], Sabine Seisel[†], Karina Elumeeva[†], Stefan Barwe[†], Sara Marti-Sanchez[Ψ], Jordi Arbiol[Ψ,Φ], Ilya Sinev[§], Beatriz Cuenya Roldan[§], Martin Muhler[‡], Wolfgang Schuhmann[†]**

† Analytical Chemistry - Center for Electrochemical Sciences (CES), Ruhr-Universität Bochum, Universitätsstr. 150, D-44780 Bochum (Germany)

‡ Laboratory of Industrial Chemistry, Ruhr-University Bochum, Universitätsstr. 150, D-44780 Bochum, Germany

§ Department of Physics, Ruhr-Universität Bochum, Universitätsstr. 150, D-44780 Bochum (Germany)

[Ψ] Catalan Institute of Nanoscience and Nanotechnology (ICN2), CSIC, and BIST, Barcelona, Catalonia, Spain [Φ] ICREA, Pg. Lluís Companys 23, 08010 Barcelona, Catalonia, Spain

AUTHOR INFORMATION

Corresponding Author

*justus.masa@rub.de

*wolfgang.schuhmann@rub.de

ABSTRACT

The modification of nickel with boron or phosphorus leads to significant enhancement of its electrocatalytic activity for the oxygen evolution reaction (OER). However, the precise role of the guest elements, B and P, in enhancing the OER of the host element (Ni) remains unclear. Herein, we present novel insight into the role of B and P in OER electrocatalysis by nickel borides and nickel phosphides. XPS data revealed that B and P induce opposite electronic effects on the surface electronic structure of Ni, thus rendering electronic structure modification or ligand effect inconsequential in explaining the origin of the OER activity enhancement. The apparent energy of activation E_a* of the OER on Ni_2P was 74.0 kJ/mole, on Ni_2B 65.4 kJ/mole, and on Ni nanoparticles 94.0 kJ/mole, thus clearly revealing that both B and P affect the intrinsic OER activity of nickel. Lattice changes, specifically, the Ni-Ni atomic order and bond distances induced by the presence of the guest atoms, seem to be the dominant factors responsible for enhanced electrocatalysis of the OER in nickel borides and nickel phosphorus.

TOC GRAPHIC

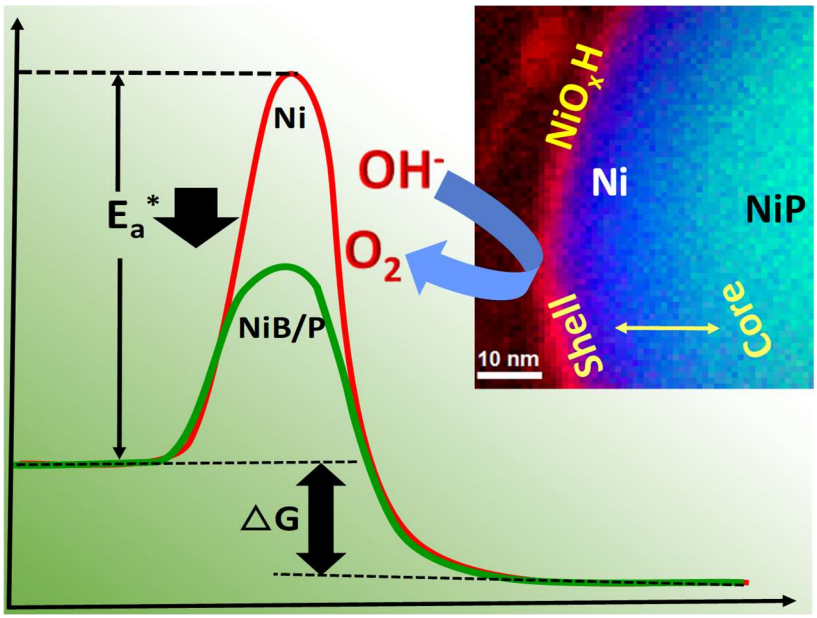

The turn of the 21st century has witnessed unprecedented pursuit of environmentally friendly and sustainable energy technologies owing to the depletion and eco-unfriendliness of the present-day energy systems and their associated contribution to global warming and climate change.[1] Renewable power-to-hydrogen production by electrochemical water splitting is one of the most promising means for storing and enhancing the energy obtained from renewable energy sources.[2] The low efficiency of the energy recovery cycle due to inefficient electrocatalysis in contemporary regenerative power-to-hydrogen, and hydrogen-to-power energy systems, coupled with the high cost of the systems due to their reliance on the costly platinum group metals (PGM) as electrocatalysts have impeded their entry to a wider market.[3] To this end, reducing the use of the PGM, or better, completely replacing them with efficient low-cost electrocatalysts can tremendously improve the competitiveness of power-to-hydrogen and hydrogen-to-power renewable energy systems.

Compounds and alloys of Co, Ni and Fe, among others, with the pnictogens, chalcogens and some metalloids,[4–8] have tremendous bonding and structural diversity[9, 10] and have recently emerged as very promising low-cost catalysts for the oxygen evolution reaction (OER) in alkaline electrolytes. Studies on these catalysts have in the past, however, focused mainly on enhancing activity through optimization of syntheses, meanwhile, the origin of enhanced electrocatalytic O_2 evolution remains unsatisfactorily explained. Additionally, the dependence of the OER activity on alloy stoichiometry and crystal structure has been reported but not adequately explained. Understanding the origin of activity enhancement in these compounds is an important step to further improve their activity and use them as models for the development of new advanced catalysts.

In this work, we present insight into the role of B and P in enhancing OER electrocatalysis by nickel, as observed in nickel phosphides and nickel borides. In nickel borides, electrons are drawn from boron towards nickel, whereas, in nickel phosphides, net electron transfer is towards phosphorus, rendering electronic structure modification inadequate to explain the origin of the OER activity enhancement. Substantially lower apparent energies of OER activation were observed when using Ni_2P and Ni_2B as OER catalysts compared to pure Ni nanoparticles. The geometric changes induced by B and P on the lattice structure of Ni, notably, the Ni-Ni bond distances, as well as the Ni-P and Ni-B bond distances, thus appear to be the decisive factors for enhanced OER activity in Ni_2B and Ni_2P.

We used semi-crystalline Ni_2B and commercial Ni_2P as model catalysts to investigate the role of B and P in promoting electrocatalytic oxygen evolution in nickel borides and nickel phosphides. Ni_2B was prepared according to a previously reported procedure[7], as described in the supporting information, while Ni_2P was a commercial sample from Sigma Aldrich. XRD analysis of Ni_2P indicates predominance of the Ni_2P phase (**Fig S1**), with minor impurities of Ni_3P and $Ni_{12}P_5$. In studying the electrocatalytic behavior of these materials, it is important to point out an often overlooked or not explicitly disclosed fact that these kind of materials tend to undergo tremendous transformation under electrochemical polarization depending on their initial state.[7] For example, the intensity of the $Ni^{2+} \rightarrow Ni^{3+}$ oxidation peak of Ni_2B increased with potential cycling up to a ~5-fold factor before a steady state was reached (**Fig.1a**). Increase in the intensity of the $Ni^{2+} \rightarrow Ni^{3+}$ oxidation peak indicates growth of a NiOOH layer and is often accompanied with increase of the OER activity. This observation stresses the necessity to apply a suitable conditioning step to the catalyst films to bring them to a steady state in order to enable accurate determination of their activity and thus a fair comparison. For all the catalysts reported

in this study, 100 conditioning CVs were applied to the electrodes prior to recording activity measurements. Fig. 1b shows linear sweep voltammograms (LSVs) of the OER in 1.0 M KOH catalyzed by Ni_2B, Ni_2P and nickel nanoparticles (Ni) for comparison. It is evident from the graphs that the presence of either B or P in Ni leads to enhanced OER electrocatalysis compared to pure Ni nanoparticles. Ni_2B exhibited better OER performance than Ni_2P when the currents were normalized with respect to geometric electrode area. The turnover frequency (*TOF*); $[TOF = i(A)/(4Fn)]$; where i is electrocatalytic current at a specific potential, F = Faraday constant and n is the number of moles of Ni in the catalyst, for O_2 evolution at 1.6 V calculated using the nominal loading of Ni was 0.017 $mol^{-1}s^{-1}$ for Ni_2B, 0.012 $mol^{-1}s^{-1}$ for Ni_2P and 6.5 x 10^{-4} $mol^{-1}s^{-1}$ for Ni, indicating that both B and P considerably enhance the inherent activity of the Ni atoms. However, the comparatively high intensity of the $Ni^{2+} \rightarrow Ni^{3+}$ peak for Ni_2B suggests that its apparently dominant activity could be due to a higher surface area and thus higher accessibility of Ni compared to Ni_2P and Ni. Normalization of the current in Fig. 1b with respect to the accessible moles (n) of Ni determined by integration $\left[n = \frac{1}{F}\frac{\int_{E1}^{E2} I dE}{\frac{dE}{dt}}\right]$ of the area under the $Ni^{2+} \rightarrow Ni^{3+}$ peak now projects Ni_2P as being more active than Ni_2B (see inset of Fig. 1b). The TOF calculated using the number of moles of electrochemically accessible Ni was 0.18 $mol^{-1}s^{-1}$ for Ni_2B, 0.959 $mol^{-1}s^{-1}$ for Ni_2P, and 0.055 $mol^{-1}s^{-1}$ for Ni. The number of moles of Ni determined by integration of the $Ni^{2+} \rightarrow Ni^{3+}$ peaks, 3.65 x 10^{-8} mol for Ni_2B, 4.2 x 10^{-9} mol for Ni_2P and 5.1 x 10^{-9} mol for Ni, were two orders of magnitude in the case of Ni_2P and Ni, and one order of magnitude for Ni_2B lower than the moles in the nominal catalyst loading, 3.9 x 10^{-7} mol for Ni_2B, 3.4 x 10^{-7} mol for Ni_2P and 4.3 x 10^{-7} mol for Ni. Thus, whereas in all the three cases not all the Ni atoms were electrochemically accessible, it is clear that the accessibility of the Ni atoms was higher in the case of Ni_2B, which might be due to a structure that favors higher

accessibility, or due to better conductivity of Ni_2B compared to Ni_2P and Ni. The Tafel slope of the OER was 57.8, 57.0 and 62.3 mV/dec on Ni_2B, Ni_2P and Ni, respectively, indicating a similar rate-limiting step on the catalysts (**Fig.1c**).

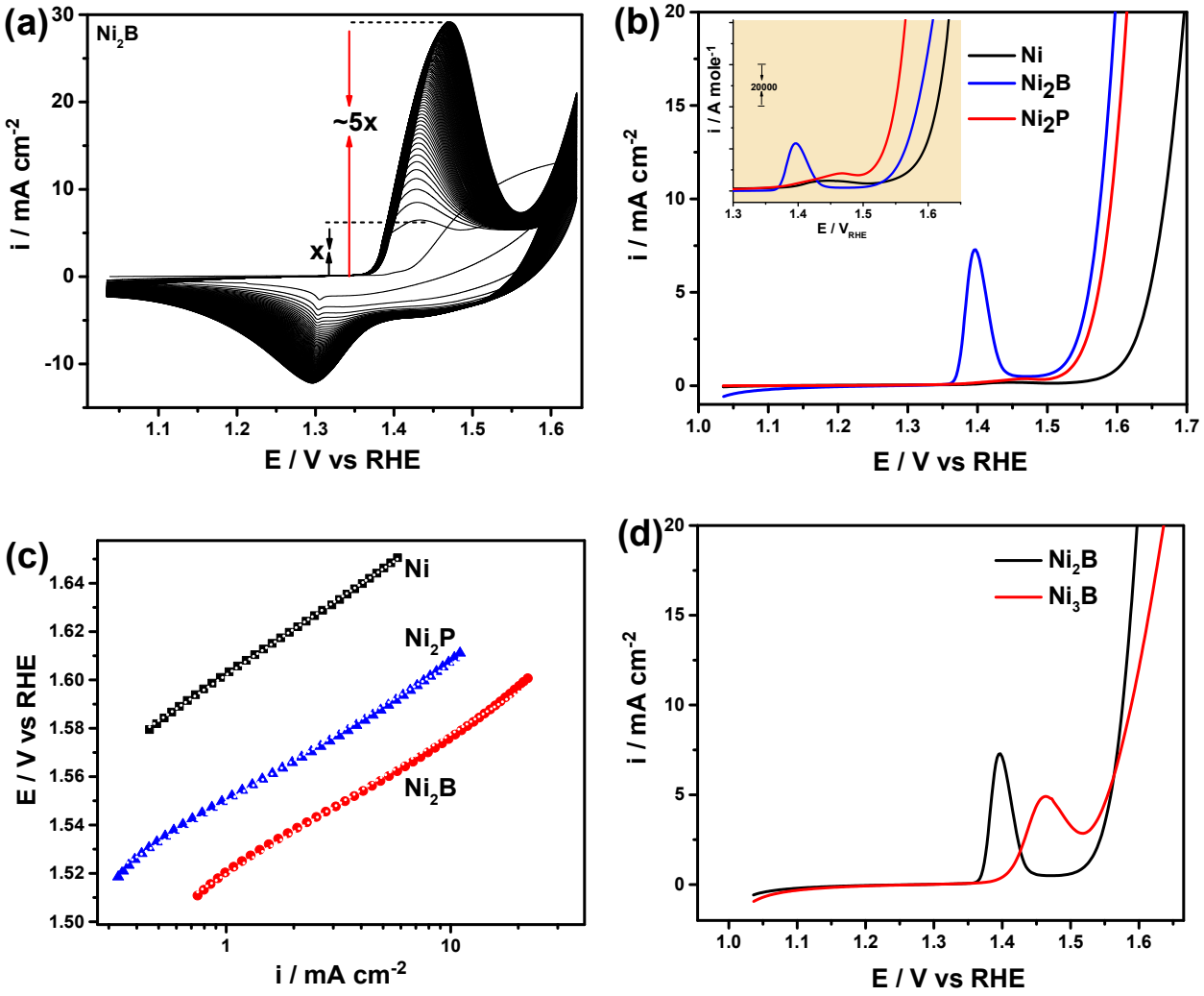

Figure 1. (a) Conditioning of a glassy carbon electrode modified with a Ni_2B film by continuous cyclic voltammetry at a scan rate of 100 mV s^{-1} in KOH (1.0 M); (b) Linear sweep voltammograms (LSVs) of Ni_2B, Ni_2P and Ni nanoparticles recorded in KOH (1.0 M) at scan rate of 10 mV s^{-1} and rotation speed of 1600 rpm (the inset shows an enlarged view of the $Ni^{2+} \rightarrow Ni^{3+}$ oxidation region); (c) Tafel plots of Ni_2B, Ni_2P and Ni; (d) LSVs of Ni_2B and Ni_3B in KOH (1.0 M) highlighting the influence of the Ni:B stoichiometry on OER activity.

The influence of the Ni:B/P stoichiometry on the OER is illustrated in **Fig. 1d** by comparison of the OER activity of Ni_2B and Ni_3B. The synthesis and characterization of Ni_3B was reported previously.[7] The Ni:B ratio apparently affects the potential for $Ni^{2+} \rightarrow Ni^{3+}$ oxidation, as indicated by a higher potential of the $Ni^{2+} \rightarrow Ni^{3+}$ oxidation peak. Both catalysts begin to evolve oxygen at about the same potential, however, the current rises more sharply in the case of Ni_2B owing to a lower Tafel slope (57.8 mV/dec) compared to that of Ni_3B (62.5 mV /dec). The OER is therefore not only affected by the presence of B but also by the Ni:B ratio in the catalyst. A similar effect has been reported for nickel phosphide based hydrogen evolution catalysts.[11]

The inability to reliably determine the TOF of the catalysts owing to non-participation of all available Ni atoms in the reaction implies that the TOF is not a decisive metric for describing the intrinsic activity of the catalysts.

The activation energy of a reaction is an intensive quantity that only depends on the inherent properties of the catalyst and is insensitive to extrinsic factors that accrue from the interaction of the electrode with the electrolyte, and to extended morphological features of the surface. We recorded the OER on Ni_2B, Ni_2P and Ni at different electrolyte temperatures from 20 ºC to 65 ºC. **Fig. 2a** shows LSVs recorded on a Ni_2P modified electrode at different electrolyte temperatures. As can be seen, the rate of O_2 evolution increased with temperature as manifested by decrease of the OER overpotential with temperature and higher electrocatalytic currents. This dependence implies that the reaction can be treated by Arrhenius kinetics to determine the activation energy of the OER on the various catalysts. However, since the OER is a multi-step reaction involving many intermediates and activation steps, with the rate-limiting step not known, we have chosen to refer to the determined activation energy as apparent energy of activation, denoted as E_a*.

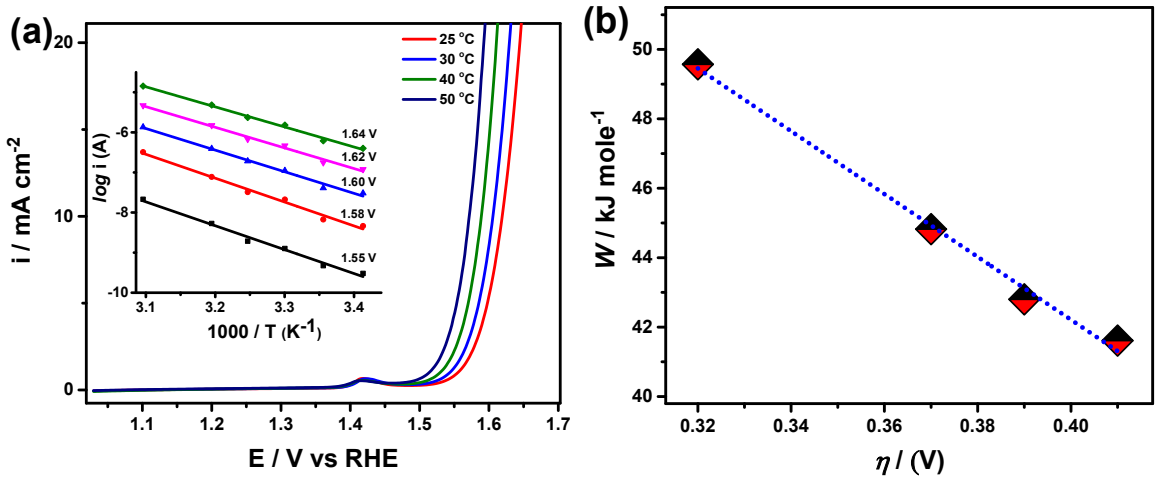

Figure 2. (a) Linear sweep voltammograms of Ni_2P with the inset showing a plot of *log i* versus *1/T* at various overpotentials, and (b) plot of total energy of activation (*W*) against OER over-potential (η) for Ni_2P.

If mass transport effects are absent, the rate of oxygen evolution should generally increase with reaction overpotential in accordance with the Butler-Volmer equation, $i = i_0 \exp^{\alpha \frac{nF(E-E_{eq})}{RT}}$; where i = current density at a specific potential (E), i_o = exchange current density, R = universal gas constant, n = number of transferred electrons, T = temperature, F = Faraday constant, E_{eq} = equilibrium potential, and α = transfer coefficient. Since increase of the reaction rate results from a decrease of the E_a, the relationship $W = E_a - \beta V$ proposed by Bowden holds,[12] where β is a measure of the proportionality and depends on the measurement conditions, E_a is the energy of activation at the equilibrium potential (E_{eq}) and W is the total energy of activation at a given potential. The corresponding Arrhenius equation takes the form $i = Ai_o e^{-W/RT}$, where i is the OER current at a specific potential (E) or overpotential ($\eta = E - E_{eq}$), and the other terms retaining the meaning defined before.

The total energy of activation (W) of the OER at a given overpotential η was thus determined from the relationship $\left|\frac{\partial(log\ i)}{\partial\left(\frac{1}{T}\right)}\right|_{\eta} = \frac{-W}{2.303R}$, by plotting *log i* versus *1/T*. *W* decreased linearly with η as shown in **Fig. 2b**. The apparent energy of activation (E_a*) at E_{eq} was obtained from the intercept of the graph at $\eta = 0$, and was 78.4 kJ mol^{-1} for Ni_2P, 65.4 kJ mol^{-1} for Ni_2B and 94.0 kJ mol^{-1} for Ni nanoparticles. A study by Bowden,[12] showed that for a given reaction, small surface impurities can significantly affect the value of α and E_a*. Since Ni_2B, Ni_2P and Ni were investigated under similar conditions, these values represent inherent properties of the respective catalysts. The guest elements (B and P) therefore obviously affect the intrinsic electrocatalytic activity of the host element (Ni).

We probed the influence of B and P on the surface electronic properties of Ni by means of XPS. **Fig. 3a** shows high-resolution XPS spectra of the Ni 2p region of Ni_2P and Ni_2B. The binding energy (BE) of the Ni $2p_{3/2}$ peak was 852.52 eV for Ni_2B and 852.30 eV for Ni_2P, translating into chemical shifts of -0.08 eV and 0.40 eV respectively, with respect to the BE of the $2p_{3/2}$ peak at 852.60 eV for pure nickel.[13] These results are consistent with the work of Okamoto et al. and others, who reported electron enrichment of Ni in the presence of boron, whereas P accepted electrons from Ni.[14–17] Therefore, the fact that B and P induce two opposite electronic effects on Ni yet both lead to enhanced electrocatalysis of the OER Ni cannot be rationalized by electronic structure modification. We recognize that there is no unified theory explaining electron transfer in metal-metalloid compounds and metallic glassy alloys and some controversy exists,[18, 19] so our inferences are confined to the experimental observations. A discuss of electron transfer theories in these compounds is outside the scope of this work.

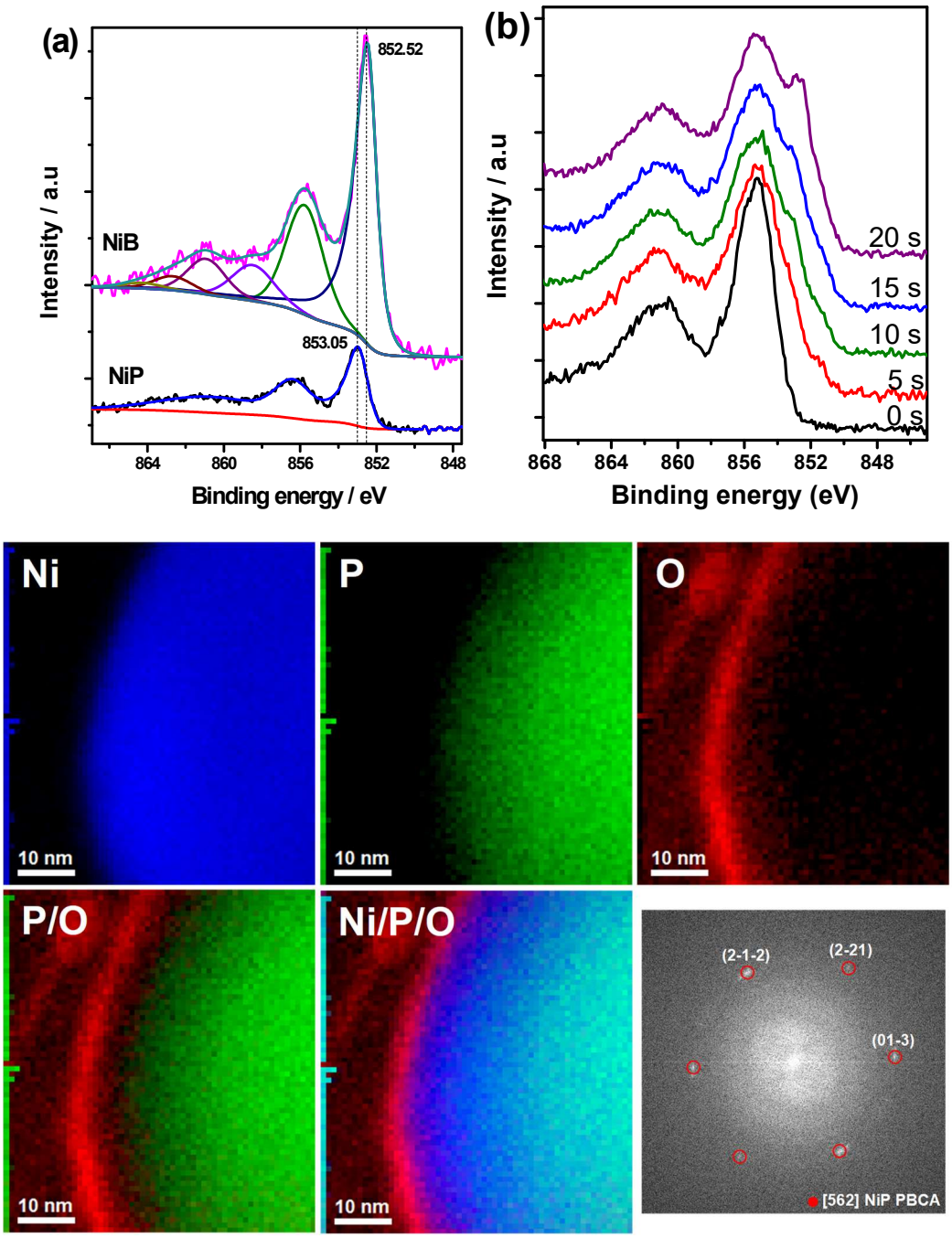

Figure 3. (a) High-resolution XPS spectra of the Ni 2p region of Ni_2B and Ni_2P; **(b)** evolution of the Ni 2p spectrum with time during Ar^+ sputtering of OER activated Ni_2B; (c) Top row: EELS elemental maps obtained on the core-shell structure of an activated NiP nanoparticle catalyst

showing the spatial distribution of Ni, P and O. Botton row: a couple of RGB composite maps combining the different elements to emphasize the core-shell structure (P/O (left) and Ni/P/O (middle)); (right) power spectrum (FFT) obtained on a HRTEM image of the same nanoparticle showing the crystal structure of the NiP.

Importantly, XPS post-mortem analysis of both Ni_2B and Ni_2P after electrochemical activation indicates that their surfaces are similar and covered with NiOOH.[7] Upon polarization, both Ni_2B and Ni_2P adopt a core-shell structure, where the surface is composed of NiOOH while the core is Ni_2P and Ni_2B. This was confirmed by XPS depth profiling by Ar^+ sputtering, which revealed increase in the Ni^0/Ni^{2+} ratio with sputtering time, and a clear increase in the intensity of the Ni $2p_{3/2}$ peak at 852.52 eV, as illustrated in **Fig. 3b** for the case of activated Ni_2B. Evidence of the core-shell structure of the activated Ni_2P catalyst is provided by the elemental intensity maps showing the spatial distribution of Ni, P and O (**Fig. 3c**), obtained by Electron Energy Loss Spectroscopy (EELS). As we can observe, Ni and P are mainly concentrated in the bulk of the particle meanwhile oxygen is on the surface. In addition, high resolution transmission electron microscopy analysis of the particles (not shown here, see SI) and the corresponding obtained power spectra (FFT) as the example shown in Fig 3c and detailed studies in SI, revealed that they have a NiP orthorhombic structure with Pbca space group.

Essentially, the modification of Ni with B or P leads to expansion of the Ni-Ni bond distance, and various Ni:B/Ni:P ratios and crystalline structures give rise to dissimilar Ni-Ni distances. As an illustration, the unit cell structures of Ni_3B, Ni_2B and NiB are presented in **Fig. 3** to show the effect of the Ni:B stoichiometry and crystal structure on the Ni-Ni bond distances. For example, the nearest Ni-Ni bond distance in Ni_2P is 2.640 Å whereas it is 2.563 Å in Ni_5P_4, both longer than 2.492 Å, the Ni-Ni bond length in pure Ni.[20] As shown in **Fig. 1d**, variation of the

Ni:B/Ni:P ratio influences the OER activity. Higher complexity in underpinning the role of B and P arises if besides variation in the lattice parameters, subtle changes in the electronic structure of the host metal accompany variation of the Ni:B/Ni:P stoichiometry.

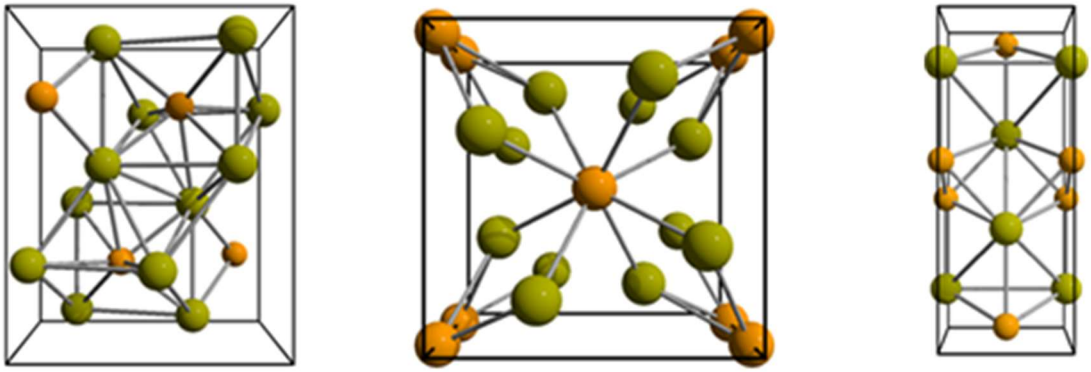

Figure 4. Unit cell structures of Ni_3B, Ni_2B and NiB showing the influence of the Ni:B ratio and crystal structure on the Ni lattice.

We previously observed that under OER conditions, surface B and P get oxidized to form their respective oxo-species, borates and phosphates.[6, 7] These species being anionic obviously introduce unique interactions at the electrode/electrolyte interface, which are inexistent on pure Ni electrodes. Therefore, in addition to deciphering the complex interplay between the electronic and geometric factors, solid understanding of the nature of electrode/electrolyte interactions, specifically, how the B and P oxo-species contribute to these interactions, and the ultimate effect on the mechanism and kinetics of the OER is imperative in order to get a holistic interpretation of the role of B and P in promoting the OER activity of Ni.

In conclusion, in nickel borides and phosphides, the guest atoms (boron and phosphorus) induce opposite electronic effects on the host atom (nickel), yet both elements bring about enhanced electrocatalysis of oxygen evolution. The origin of OER activity enhancement cannot

therefore be rationalized by electronic structure modification. The presence of B or P leads to a decrease of the energy of activation of the OER, indicating intrinsic changes in the electrocatalytic properties of nickel. Changes in the lattice structure induced by the presence of B or P, specifically, the atomic order of the Ni atoms, and the Ni-Ni bond distances, therefore seem to be the dominant factors for electrocatalytic enhancement of the OER in nickel borides and nickel phosphides.

Materials and methods

Catalyst synthesis

Nickel phosphide (Ni_2P) powder (~100 mesh, 98%) and nickel nanopowder were from Sigma Aldrich. Semi-crystalline Ni_2B was prepared by reaction of a solution of $NiCl_2$ (1.0 M) with $NaBH_4$ (1.0 M) in NaOH (1.0) followed by annealing at 300 ºC under argon for 2 hours.[7]

XRD and XPS characterization

XRD measurements were performed using a PANalytical theta-theta powder diffractometer equipped with a Cu-K α-radiation source.

XPS measurements were carried out in an ultra-high vacuum set-up (UHV) equipped with a high resolution Gammadata-Scienta SES 2002 analyzer. A monochromatic Al $K\alpha$ X-ray source (1486.3 eV; anode operating at 14.5 eV and 30.5 mA) was used as incident radiation and a pass energy of 200 eV was chosen resulting in an energy resolution better than 0.5 eV. Charging effects were compensated using a flood gun. Binding energies were calibrated by positioning the main C 1s peak at 284.5 eV.

Electrochemical characterization

The electrochemistry measurements were performed in a glass cell with a heated jacket. Glassy carbon electrodes (0.1134 cm^2) modified by drop coating 5.0 µL suspensions of the catalysts (5.0 mg mL^{-1}) in water, ethanol and Nafion (49:49:2 v/v%) were used as the working electrodes. The catalyst loading in each case was 0.210 mg cm^{-2}. A platinum mesh enclosed in a glass tube filled with the electrolyte and separated from the working electrode by means of a glass frit was used as the counter electrode, while the reference electrode was a Ag/AgCl/3 M KCl electrode separated from the heated electrolyte by means of a Luggin capillary. The measurements were performed using an Autolab Potentiostat/Galvanostat, PGSTAT128N (Metrohm). All measured potentials were iR corrected and converted to the reversible hydrogen electrode (RHE) scale according to:

$E_{RHE} = E_{Ag/AgCl} + 0.059pH + E^o_{Ag/AgCl}$; where $E_{Ag/AgCl}$ is the potential measured by the Ag/AgCl reference electrode and $E^o_{Ag/AgCl}$ is the potential of the Ag/AgCl with respect to the standard hydrogen electrode. The pH of the electrolyte was measured using a pH meter specifically designed for high pH electrolyte, the pH-meter CP-411 by Dr. Kornder. For the used 1.0 M KOH, the measured pH was 13.99, similar to the calculated $pH = 14 + \log[OH^-] + \log \gamma$) using the activity coefficient of 1.0 M KOH at 25 ºC ($\gamma = 0.978$). [21] The OER activity was recorded by linear sweep voltammetry from 1.0 V to 1.8 V at a scan rate of 10 mV s^{-1} in 1.0 M KOH with electrode rotation at 1600 rpm.

Transmission Electron Microscopy

High-resolution Transmission Electron Microscopy (HRTEM) and scanning TEM (STEM) studies were carried out using a field emission gun FEI Tecnai F20 microscope at 200 kV with a point-to-point resolution of 0.19 nm. High angle annular dark-field (HAADF) STEM was

combined with electron energy loss spectroscopy (EELS) in the Tecnai microscope by using a GATAN QUANTUM filter.

ASSOCIATED CONTENT

AUTHOR INFORMATION

justus.masa@rub.de, wolfgang.schuhmann@rub.de, http://www.rub.de/elan

Notes

"The authors declare no competing financial interest."

ACKNOWLEDGMENT

The authors acknowledge support by the BMBF in the framework of the project "NEMEZU" (03SF0497B). SMS acknowledges funding from "Programa Internacional de Becas "la Caixa"-Severo Ochoa". JA and SMS acknowledge funding from Generalitat de Catalunya 2017 SGR 327 and the Spanish MINECO project VALPEC (ENE2017-85087-C3). ICN2 acknowledges support from the Severo Ochoa Programme (MINECO, Grant no. SEV-2013-0295) and is funded by the CERCA Programme / Generalitat de Catalunya. Part of the present work has been performed in the framework of Universitat Autònoma de Barcelona Materials Science PhD program.

References

1. Chu, S.; Majumdar, A. Opportunities and challenges for a sustainable energy future. *Nature* **2012,** *488* (7411), 294–303.

2. Götz, M.; Lefebvre, J.; Mörs, F.; McDaniel Koch, A.; Graf, F.; Bajohr, S.; Reimert, R.; Kolb, T. Renewable Power-to-Gas: A technological and economic review. *Renew. Energ* **2016,** *85*, 1371–1390.

3. Zeng, K.; Zhang, D. Recent progress in alkaline water electrolysis for hydrogen production and applications. *Prog. Energ. Combust* **2010,** *36* (3), 307–326.

4. Anantharaj, S.; Ede, S. R.; Sakthikumar, K.; Karthick, K.; Mishra, S.; Kundu, S. Recent Trends and Perspectives in Electrochemical Water Splitting with an Emphasis on Sulfide, Selenide, and Phosphide Catalysts of Fe, Co, and Ni: A Review. *ACS Catal.* **2016,** *6* (12), 8069–8097.

5. Masa, J.; Weide, P.; Peeters, D.; Sinev, I.; Xia, W.; Sun, Z.; Somsen, C.; Muhler, M.; Schuhmann, W. Amorphous Cobalt Boride (Co_2B) as a Highly Efficient Nonprecious Catalyst for Electrochemical Water Splitting: Oxygen and Hydrogen Evolution. *Adv. Energy Mater.* **2016**, *6* (6), 1502313.

6. Masa, J.; Barwe, S.; Andronescu, C.; Sinev, I.; Ruff, A.; Jayaramulu, K.; Elumeeva, K.; Konkena, B.; Roldan Cuenya, B.; Schuhmann, W. Low Overpotential Water Splitting Using Cobalt–Cobalt Phosphide Nanoparticles Supported on Nickel Foam. *ACS Energy Lett.* **2016,** *1* (6), 1192–1198.

7. Masa, J.; Sinev, I.; Mistry, H.; Ventosa, E.; La Mata, M. de; Arbiol, J.; Muhler, M.; Roldan Cuenya, B.; Schuhmann, W. Ultrathin High Surface Area Nickel Boride (Ni_xB) Nanosheets as Highly Efficient Electrocatalyst for Oxygen Evolution. *Adv. Energy Mater.* **2017,** *7* (17), 1700381.

8. Suen, N.-T.; Hung, S.-F.; Quan, Q.; Zhang, N.; Xu, Y.-J.; Chen, H. M. Electrocatalysis for the oxygen evolution reaction: recent development and future perspectives. *Chem. Soc. Rev.* **2017,** *46* (2), 337–365.

9. Carenco, S.; Portehault, D.; Boissière, C.; Mézailles, N.; Sanchez, C. Nanoscaled metal borides and phosphides: recent developments and perspectives. *Chem. Rev.* **2013,** *113* (10), 7981–8065.

10. Chen, J.-H.; Whitmire, K. H. A structural survey of the binary transition metal phosphides and arsenides of the d -block elements. *Coord. Chem. Rev.* **2018,** *355*, 271–327.

11. Kucernak, A. R. J.; Naranammalpuram Sundaram, V. N. Nickel phosphide: The effect of phosphorus content on hydrogen evolution activity and corrosion resistance in acidic medium. *J. Mater. Chem. A* **2014,** *2* (41), 17435–17445.

12. Bowden, F. P.; Rideal, E. K. The Electrolytic Behaviour of Thin Films. Part I. Hydrogen. *Proc. R. Soc. A* **1928,** *120* (784), 59–79.

13. Grosvenor, A. P.; Biesinger, M. C.; Smart, R. S.; McIntyre, N. S. New interpretations of XPS spectra of nickel metal and oxides. *Surf. Sci* **2006,** *600* (9), 1771–1779.

14. Okamoto, Y.; Nitta, Y.; Imanaka, T.; Teranishi, S. Surface characterisation of nickel boride and nickel phosphide catalysts by X-ray photoelectron spectroscopy. *J. Chem. Soc., Faraday Trans. 1* **1979,** *75* (0), 2027–2039.

15. Tyan, Y. S.; Toth, L. E.; Chang, Y. A. Low temperature specific heat study of the electron transfer theory in refractory metal borides. *J. Phys. Chem. Solids* **1969,** *30* (4), 785–792.

16. Greenwood, N. N.; Parish, R. V.; Thornton, P. Metal borides. *Q. Rev., Chem. Soc.* **1966,** *20* (3), 441.

17. Li, H.; Li, H.; Dai, W.-L.; Wang, W.; Fang, Z.; Deng, J.-F. XPS studies on surface electronic characteristics of Ni–B and Ni–P amorphous alloy and its correlation to their catalytic properties. *Appl. Surf. Sci* **1999,** *152* (1-2), 25–34.

18. Chen, Y. Chemical preparation and characterization of metal–metalloid ultrafine amorphous alloy particles. *Catalysis Today* **1998,** *44* (1-4), 3–16.

19. Shveikin, G. P.; Ivanovskii, A. L. The chemical bonding and electronic properties of metal borides. *Russ. Chem. Rev.* **1994,** *63* (9), 711–734.

20. Wang, Y.; Kong, B.; Zhao, D.; Wang, H.; Selomulya, C. Strategies for developing transition metal phosphides as heterogeneous electrocatalysts for water splitting. *Nano Today* **2017,** *15*, 26–55.

21. Knobel, M. The activities of the ions of potassium hydroxide in aqueous solution. *J. Am. Chem. Soc.* **1923,** *45* (1), 70–76.